Surface structure and dipole moments of RbI(001) determined by high-resolution medium-energy ion scattering

2001 J. Phys.: Condens. Matter 13 9835

(http://iopscience.iop.org/0953-8984/13/44/301)

INSTITUTE OF PHYSICS PUBLISHING JOURNAL OF PHYSICS: CONDENSED MATTER

J. Phys.: Condens. Matter **13** (2001) 9835–9845 PII: S0953-8984(01)25454-X

Surface structure and dipole moments of RbI(001) determined by high-resolution medium-energy ion scattering

T Okazawa, Y Hoshino, T Nishimura and Y Kido[1]

Department of Physics, Ritsumeikan University, Kusatsu, Shiga-ken 525-8577, Japan

E-mail: ykido@se.ritsumei.ac.jp

Received 4 June 2001, in final form 3 September 2001
Published 19 October 2001
Online at stacks.iop.org/JPhysCM/13/9835

Abstract

The surface structure of RbI(001) was determined directly by means of medium-energy ion scattering (MEIS) with a monolayer depth resolution. The rumpled surface structure determined here was compared with semi-classical shell-model calculations. On the basis of a simple model regarding the lattice site ion as a point charge accompanied by a dipole moment, we evaluated the dipole moments of the top- and second-layer I^- and Rb^+ ions self-consistently from the relaxed lattice positions determined by means of MEIS and from the polarizabilities estimated systematically from experimental refraction data. The balance between a short-range force and a long-range coulombic one determined the equilibrium positions of the top- and second-layer ions; these are consistent with those derived by means of MEIS within the experimental uncertainties of 0.02 Å. This indicates that the polarizablities derived from the refraction data and the interatomic (short-range) potentials of the Born–Mayer type are applicable.

1. Introduction

Medium-energy ion scattering (MEIS) provides a powerful tool for determining directly near-surface and interface structures [1–3]. Recently, MEIS with a monolayer depth resolution has been applied to the analysis of metal silicide/Si interfaces, surface structures of metals and oxides, and initial oxidation of Si surfaces [4–7]. The notable point of the ion scattering analysis is its reliability due to the simple and well-established principle and direct observation in real space, in contrast to the diffraction (momentum-space) methods using electrons and x-rays.

[1] Author to whom any correspondence should be addressed. Telephone: +81-77-561-2710; fax: +81-77-561-2657.

In the present work, we first determined the surface structure of RbI(001) by means of high-resolution MEIS. As is well known, alkali halide crystals have strongly rumpled surface structures due to the dipole moment of negative ions being considerably larger than that of positive ions [8]. Our toroidal electrostatic analyser (ESA) for MEIS has an excellent energy resolution ($\Delta E/E = 9 \times 10^{-4}$) and thus allows a layer-by-layer analysis [9–11]. As shown later, it resolved the scattering components from the top- and second-layer Rb^+ and I^- ions. Using the ion shadowing effect [10, 11], we determined the heights of the top-layer I^- and Rb^+ ions from the second-layer I^- and Rb^+ ions. Thus the surface relaxation and the rumplings of the top and second layers were deduced. Then, on the basis of the simple model wherein the lattice site ion is regarded as an elemental point charge ($\pm e$) accompanied by a dipole moment, the local electric fields and the dipole moments for the top- and second-layer Rb^+ and I^- ions are derived self-consistently. It must be noted that for the ions in deeper layers, the electric fields generated by the surrounding ions are cancelled out and thus no dipole moments are induced. In order to study the lattice dynamics at surfaces, we need a reliable short-range pair potential. Previously, some pair potentials of the Born–Mayer type [12–14] were proposed for alkali halide crystals. We checked whether the forces were balanced between the short-range force and a long-range coulombic one at the relaxed lattice positions determined by MEIS.

As regards the structures and dipole moments of ions near the alkali halide surfaces, some theoretical predictions have been made based on the semi-classical shell models [12, 15, 16]. Recently, first-principles local density calculations were performed to deduce the polarizabilities of alkali halide crystals [17, 18]. It is impossible to determine experimentally the polarizabilities of the positive and negative ions separately by optical methods applied to the dielectric response. However, individual polarizabilities can be estimated systematically from experimental data using the Clausius–Mossotti relation. Up to the present, optimized surface structures of alkali halide crystals based on *ab initio* molecular dynamics simulation have not been calculated, because this needs many more plane waves as the basis functions than simulation for metals and semiconductors. In addition, there are no experimental reports on the structures and the dipole moments of near-surface ions for alkali halide crystals. The present study provides useful experimental data on the structure and dipole moments of the RbI(001) surface and makes it possible to evaluate the accuracies of the theoretical models applied to ionic crystals.

2. Experiment

The RbI crystal has a NaCl-type structure with lattice constant of 7.342 Å at room temperature. RbI(001) crystals with purity better than 99.9% were purchased from the Crystal Growth Laboratory of the University of Utah. A crystal with a size of $14 \times 14 \times 1$ mm^3 was cleaved in the atmosphere with a razor-blade and then immediately installed into the ion scattering chamber evacuated to ultrahigh vacuum (UHV: 2×10^{-10} Torr). It is a crucial that the crystal is cut carefully, to ensure that there is no surface damage or distortion. The sample was heated to 100–150 °C for 5 min in the UHV chamber and a clean surface without C and O contamination was confirmed by Auger electron and ultraviolet photoelectron spectroscopies, respectively. In order to avoid the charge-up effect, the sample surface was covered with thin Al foils except for a small ion-irradiation area with a size of about 4×8 mm^2. The absence of charging was confirmed by the slope and position of the front edge in the MEIS spectra from I atoms.

The specification and performance of our toroidal ESA were described elsewhere [9]. Figure 1 shows a typical MEIS spectrum for 80 keV He^+ ions incident along the [001] axis of RbI(001) and backscattered to 100°. Our toroidal ESA resolves the scattering components from

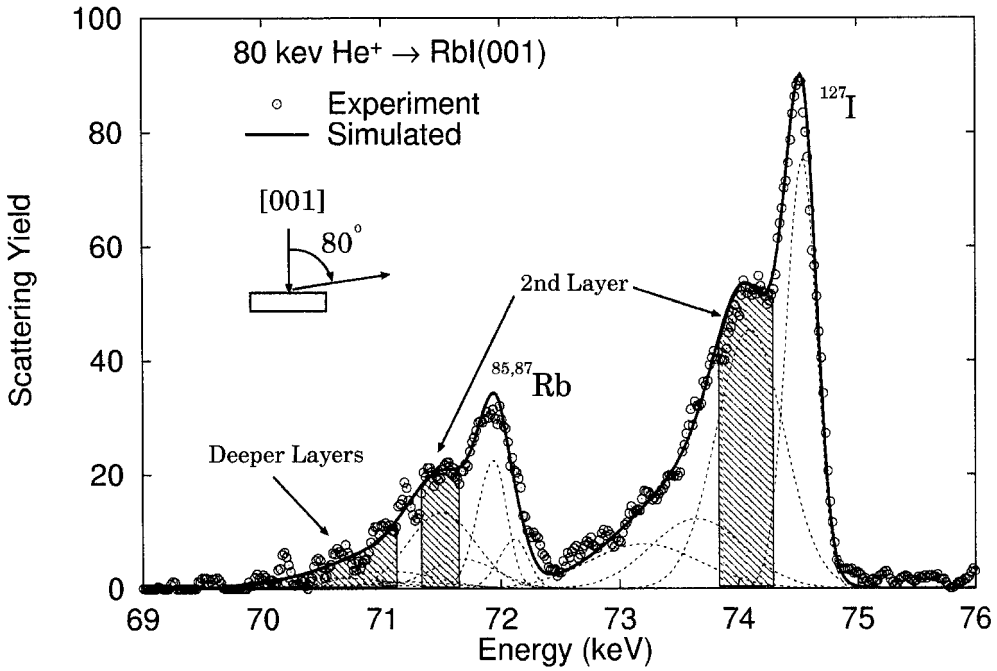

Figure 1. The observed MEIS spectrum (open circles) for 80 keV He^+ ions incident along the [001] axis of RbI(001) and backscattered to 100°. The dashed and solid curves are the deconvoluted and total MEIS spectra, respectively, best fitted to the observed one. These energy spectra were simulated assuming the energy resolution $\Delta E/E = 1 \times 10^{-3}$, stopping power $S(E) = 1.4S_Z(E)$ ($S_Z(E)$: Ziegler's stopping power; E: energy), and straggling $\Omega^2 = 0.25\Omega_B^2$ (Ω_B: Bohr straggling). The isotope abundances of ^{85}Rb (72%), ^{87}Rb (28%), and ^{127}I (100%) were taken into account.

the top- and second-layer Rb^+ and I^- ions. The dashed and solid curves are the deconvoluted Gaussian distributions (from the top down to the fourth layer, ^{127}I (100%), ^{85}Rb (72%), ^{87}Rb (28%)), and total MEIS spectrum, respectively, best fitted to the observed one. If one assumes the scattering component from each layer to be a slightly asymmetric Gaussian shape, the best-fitted spectrum is obtained by choosing the system energy resolution ($\Delta E/E$) of 1×10^{-3}, the stopping power of $1.4S_Z$ (S_Z: Ziegler's stopping power), and the energy straggling of $0.25\Omega_B^2$ (Ω_B^2: Bohr straggling). The uncertainties of these fitting parameters are estimated to be roughly $\pm 10\%$. The normalized scattering yields derived from the above best fit for the top-, second-, third-, and fourth-layer ions are 1.0, 1.2, 0.4, and 0.3, respectively. Such large values for the second-, third-, and fourth-layer ions are responsible for a strong focusing effect in the outgoing path (almost parallel to but slightly deviating from the [601] axis) and for considerable thermal vibration amplitudes (0.16–0.20 Å) due to the small Debye temperature of RbI (115 K).

3. Results and discussion

First, we determine the heights of the top-layer I^- and Rb^+ ions measured from the second-layer I^- ions. In this case, two energy windows were set for the scattering components from the second-layer I^- ions and from the deeper-layer ions (see figure 1, shaded areas). Then the angular scans were performed for the above two scattering components around the [101] axis

in the $(0\bar{1}0)$ plane and around the [111] axis in the $(1\bar{1}0)$ plane. The former angular scan gives the height of the top-layer I^- ions and the latter that of the top-layer Rb^+ ions scaled from the second-layer I^- ions. If we set an energy window for the scattering component from the second-layer Rb^+ ions (see figure 1, shaded area), the heights of the top-layer I^- and Rb^+ ions scaled from the second-layer Rb^+ ions are determined in the same manner.

Figure 2 indicates the angular scan spectra around the [101] axis in the (010) plane (left) and those around the [111] axis in the $(0\bar{1}0)$ plane (right) for the scattering components from the second-layer I^- ions and from the deeper-layer ions. The scattering angle was fixed at 80° and 68° for the polar scans around the [101] and [111] axis, respectively. We confirmed by Monte Carlo simulations that no blocking and focusing effects occur in such scattering geometries. It is known that there is no surface reconstruction on the (001) surface of NaCl-type crystal owing to its highly symmetric nature. The angles giving the scattering yield minima were determined by an appropriate polynomial fitting [10]. From the angular shifts indicated in the figures, the heights of the top-layer I^- and Rb^+ ions above the second-layer I^- ions were derived as 3.679 ± 0.01 and 3.595 ± 0.01 Å, respectively, by the simple triangulation method [10, 11]. This means that the interlayer distance of the top I^- and Rb^+ planes scaled from the second I^- plane are expanded by +0.008 Å and −0.076 Å, respectively, compared with the bulk interlayer distance d_{bulk} (3.671 Å at room temperature (RT)).

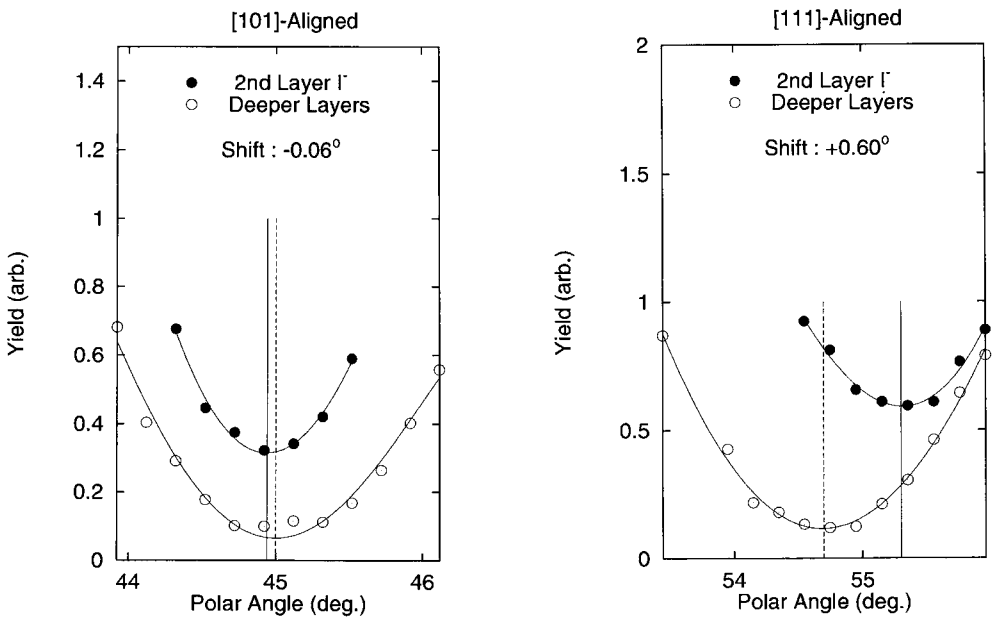

Figure 2. Angular scan spectra for 80 keV He^+ ions incident around the [101] axis in the (010) plane (left) and around the [111] axis in the $(1\bar{1}0)$ plane (right). The scattering angle was fixed at 80° and 68° for polar scans around the [101] and [111] axis, respectively. Full and open circles denote the scattering components from second-layer I^- ions and from deeper-layer ions, respectively. The solid and dashed lines indicate the angles giving the scattering yield minima determined by a polynomial curve fitting.

Figure 3 shows the angular scan spectra around the [101] axis in the (010) plane (left) and those around the [111] axis in the $(0\bar{1}0)$ plane (right) for the scattering components from the second-layer Rb^+ ions and from the deeper-layer ions. In the same way as described above, the heights of the top-layer I^- and Rb^+ ions measured from the second-layer Rb^+ ions were

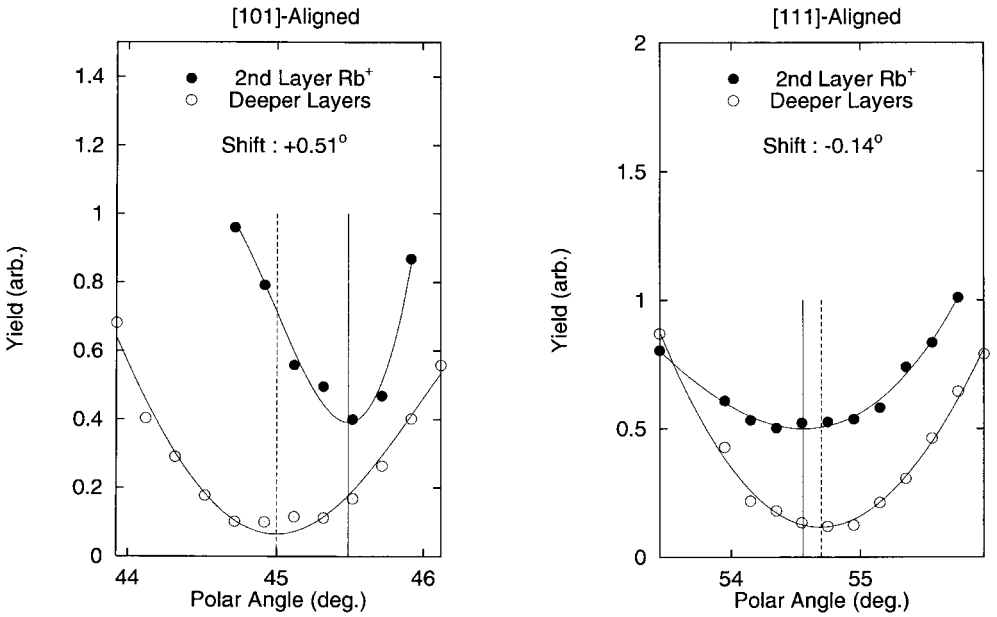

Figure 3. Angular scan spectra for 80 keV He^+ ions incident around the [101] axis in the (010) plane (left) and around the [111] axis in the $(1\bar{1}0)$ plane. The scattering angle was fixed at 80° and 68° for polar scans around the [101] and [111] axis, respectively. Full and open circles denote the scattering components from second-layer Rb^+ ions and from deeper-layer ions, respectively. The key to the symbols used is the same as that for figure 2.

deduced to be 3.695 ± 0.02 and 3.606 ± 0.02 Å, respectively. The above two values indicate that the second-layer Rb^+ ions are located below the second-layer I^- ions by 0.015 Å and 0.011 Å, respectively. This small deviation indicates good accuracy of the present analysis. Now, we take the average value of 0.013 Å.

Here, we define the surface relaxation (ε) and the rumpling of the top ($\Delta\varepsilon_1$) and second ($\Delta\varepsilon_2$) layers by the following relations (see figure 4):

$$\varepsilon = (d_{12} - d_{bulk})/d_{bulk} \times 100\% \tag{1}$$

$$\Delta\varepsilon_1 = (d_{-\mathrm{I}} - d_{+\mathrm{I}})/d_{bulk} \times 100\% = (d_{-\mathrm{R}} - d_{+\mathrm{R}})/d_{bulk} \times 100\% \tag{2}$$

$$\Delta\varepsilon_2 = (d_{-\mathrm{R}} - d_{-\mathrm{I}})/d_{bulk} \times 100\% = (d_{+\mathrm{R}} - d_{+\mathrm{I}})/d_{bulk} \times 100\% \tag{3}$$

where $d_{-\mathrm{I}}$ and $d_{+\mathrm{I}}$ are the heights of the top-layer I^- and Rb^+ ions above the second-layer I^- ions, respectively, and $d_{-\mathrm{R}}$ and $d_{+\mathrm{R}}$ are the heights of the top-layer I^- and Rb^+ ions above the second-layer Rb^+ ions, respectively. The average interlayer distance between the top and second layers is denoted by d_{12} $(=(d_{-\mathrm{I}} + d_{+\mathrm{I}} + d_{-\mathrm{R}} + d_{+\mathrm{R}})/4)$. Then the surface relaxation and rumpling of the top and second layers are deduced as $-(0.75 \pm 0.4)\%$, $+(2.29 \pm 0.4)\%$, and $+(0.35 \pm 0.5)\%$, respectively. The minus sign for the relaxation means contraction of the interlayer distance compared with the bulk interlayer distance (d_{bulk}) and the plus sign for the rumpling indicates the displacement of negative ions toward the vacuum side relative to the positive ions in the same atomic plane.

In table 1, the present result is compared with those given by the shell models [12, 15, 16]. It also includes the calculations obtained from molecular dynamics (MD) simulations performed under two different conditions: (I) for the interatomic potential and dipole moments used in reference [12]; and (II) for the interatomic potential proposed in reference [14] and the dipole

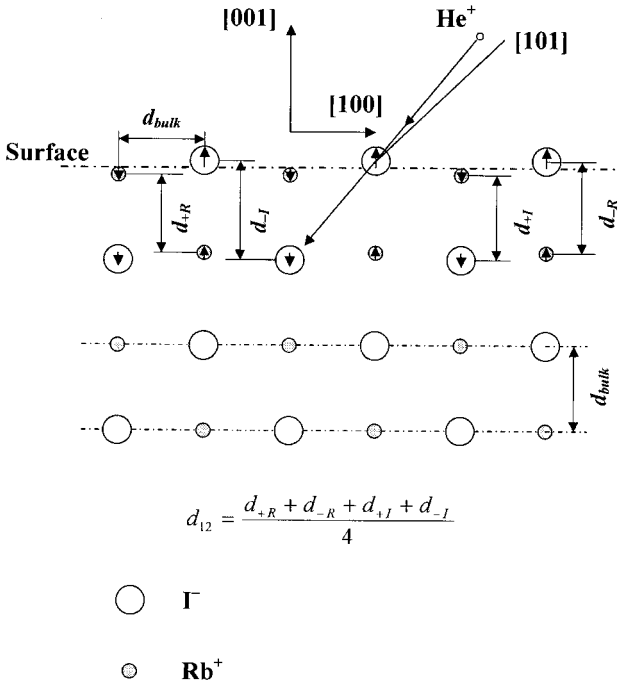

Figure 4. A schematic side view of the RbI(001) surface seen from the [010] axis. Arrows indicate the direction of the dipole moments.

Table 1. Surface relaxation (ε) and rumpling ($\Delta\varepsilon$) determined by MEIS and by the shell models [11, 14, 15]. The subscript 1 or 2 denotes the top or second layer, respectively. The plus sign for the relaxation values denotes the displacement toward the vacuum side and the plus sign for the rumpling values means the displacement of I^- ions toward the vacuum side relative to Rb^+ ions. The numbers in the square brackets are references.

	ε (%)	$\Delta\varepsilon_1$ (%)	$\Delta\varepsilon_2$ (%)
Shell model [12]	−1.41	+ 3.61	−1.80
Shell model [15]	−1.98	+ 4.18	
Shell model [16]	−1.2	+ 11.2	−6.08
Present MEIS	-0.75 ± 0.4	$+2.29 \pm 0.4$	$+0.35 \pm 0.5$
MD (I) [12]	−2.35	+ 4.16	−2.57
MD (II) [14]	−1.80	+ 3.11	−1.14

moments (top and second layers: determined by MEIS; deeper layers: neglected). For details of the MD simulation, we refer the reader to the literature [10, 19]. Significant discrepancies are seen between the present MEIS result and the predictions of the shell models. This suggests inaccuracies of these semi-classical shell-model calculations. In the above shell model, Benson and Claxton [12] introduced a distortion energy for each layer which is expressed as a function of the displacements and dipole moments of the ions in this layer. The equilibrium configuration was determined by equating to zero the first derivatives of the distortion energy for each layer independently. Such oversimplified treatment possibly led to the inaccurate result. In fact, the MD simulation (I) using the same interatomic potential and dipole moments disagrees with the shell-model calculation [12] (see table 1). The present relaxation value is increased by +0.33% compared with the previous MEIS result (−1.08%) [10]. Here, we must note that in

the previous analysis, the heights of the top-layer ions were scaled from the second-layer I^- ions only and the second-layer rumpling was neglected.

From the displacements of the top- and second-layer ions from the unrelaxed (bulk-like) lattice positions, we can deduce their dipole moments self-consistently. The dipole moment of an ion i in the nth layer is given by

$$\mu_n^i = \alpha^i \sum_j E_{total}(r_{ij}) \tag{4}$$

where α^i is the polarizability of the ion i and $E_{total}(r_{ij})$ is the total electric field induced at the position of the ion i by the point charge e_j and the dipole moment μ_m^j. Here, r_{ij} is the position vector of the jth ion relative to the ith. The electric field induced by the surrounding point charges $\sum_j E_p(r_{ij})$ was calculated by the modified Ewald method for a laminar structure [20]. In the case of the electric field generated by dipole moments $\sum_j E_d(r_{ij})$, we performed the summation over 24×24 ions in the lateral plane and neglected the contribution from the underlying layers, as a first approximation. In fact, the deeper the lattice site positions, the smaller the electric fields due to the surrounding point charges. First, the total electric field at the ion i in the top layer is calculated assuming appropriately the dipole moments of the top-layer I^- ion (μ_1^-) and Rb^+(μ_1^+). Then the dipole moment of the top-layer ions is deduced from equation (4) employing an appropriate polarizability $\alpha^{\pm}$. Thus, we can derive the dipole moments self-consistently. Figure 5 shows the contour plots of equi-inconsistency (%) for

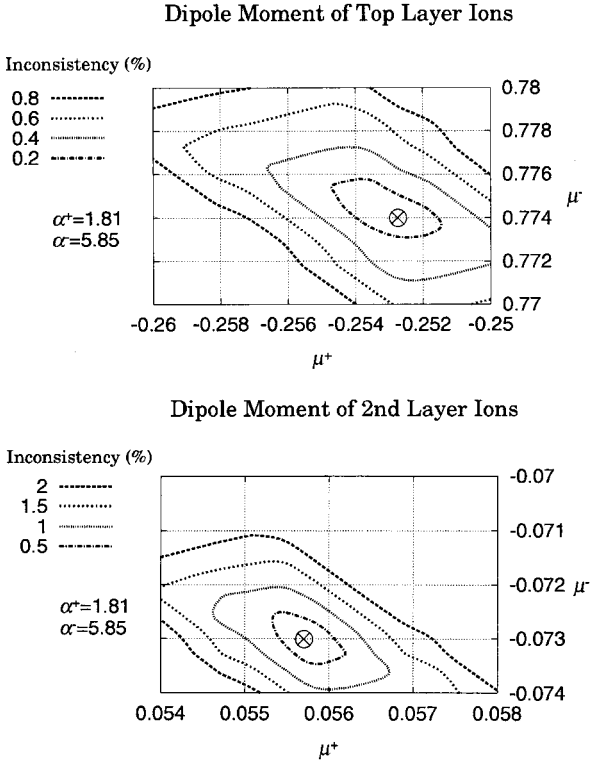

Figure 5. Contour plots of equi-inconsistency (%) for the dipole moments of the top-layer (upper) and second-layer (lower) ions. The final self-consistent values are indicated by the symbol ⊗ (see table 2).

Table 2. Dipole moments (in Debye units: 10^{-18} esu cm) derived from the rumpled surface structures. The superscript + or − denotes positive or negative ions and the plus sign for μ indicates the dipole vector directed to the vacuum side parallel to the surface normal. The values with asterisks denote corrected ones. The numbers in the square brackets indicate the references.

	α^+ (Å^3)	α^- (Å^3)	μ_1^+	μ_1^-	μ_2^+	μ_2^-
Shell model [11]	1.81 [11]	5.85 [11]	−0.249	+ 0.890	+ 0.048	−0.265
Present MEIS	1.81 [11]	5.85 [11]	−0.253	+ 0.774	+ 0.0556	−0.0730
			−0.258*	+ 0.784*	+ 0.0562*	−0.0740*
	1.38 [17]	6.95 [17]	−0.212	+ 0.853	+ 0.0455	−0.0753
	1.80 [20]	6.20 [20]	−0.264	+ 0.821	+ 0.0584	−0.0800
	1.71 [21]	6.29 [21]	−0.253	+ 0.824	+ 0.0554	−0.0783

μ_1^+ and μ_1^- (upper) and for μ_2^+ and μ_2^- (lower). The self-consistent values indicated by the cross symbol ($\otimes$) are −0.253 (μ_1^+), +0.774 (μ_1^-), +0.0556 (μ_2^+), and −0.0730 (μ_2^-) in Debye units (10^{-18} esu cm). In order to improve the accuracy, we performed the contour plots again considering the second-layer dipole moments. The correction is very small, less than 2%. In the above calculations, we employed the polarizabilities of $\alpha^+ = 1.81$ Å^3 and $\alpha^- = 5.85$ Å^3, which were deduced using equation (4) from the displacements and dipole moments predicted by the shell model [12]. These values are consistent with those ($\alpha^+ = 1.80$ Å^3 [21], 1.71 Å^3 [22]; $\alpha^- = 6.20$ Å^3 [21], 6.29 Å^3 [22]) determined systematically by experimental refraction data assuming the Clausius–Mossotti relation. Table 1 shows the dipole moments determined from the rumpled surface structure of RbI(001) assuming different polarizabilities [12, 18, 21, 22]. In all cases, the dipole moment of the top-layer I^- ions is more than three times that of the top-layer Rb^+ ions and the dipole moments of the second-layer ions are considerably reduced.

Now, we consider the force balance at the relaxed lattice positions determined by MEIS. Here, interatomic potentials of the Born–Mayer type [12–14] are employed. The short-range interactions ($V_S(r)$) between two neutral atoms are given by the following form:

$$V_S(r_{ij}) = A\exp[-r_{ij}/\rho] - C/r_{ij}^6 - D/r_{ij}^8 \tag{5}$$

where the first term corresponds to a repulsive potential and the second and third ones are effective van der Waals interactions between two dipoles induced by a fluctuation of charge distributions, respectively. This short-range interaction was taken into account for the first- and second-nearest neighbours only. The long-range coulombic potential between two ions i and j having charges e_i and e_j and dipole moments μ_i and μ_j is expressed by

$$V_L(r_{ij}) = e_ie_j/r_{ij} - e_i(r_{ij}\mu_j)/r_{ij}^3 + e_j(\mu_i r_{ij})/r_{ij}^3 - 3(\mu_i r_{ij})(\mu_j r_{ij})/r_{ij}^5 + (\mu_i\mu_j)/r_{ij}^3. \tag{6}$$

The first term denotes the interaction between point charges e_i and e_j and the second and third terms are the interaction between point charge e_i and the electric field due to dipole μ_j, and the interaction between dipole μ_i and the electric field generated by point charge e_i, respectively. The interaction between dipoles μ_i and μ_j corresponds to the fourth and fifth terms. The dipole–dipole interaction was neglected in the present analysis because of its small contribution (three orders of magnitude lower than the first term in equation (6)). The total potential energy is expressed as the sum of the short-range pair potential $V_S(r_{ij})$ and the long-range coulombic one $V_L(r_{ij})$. Figure 6(a) shows the total potential energies for the top-layer Rb^+ and I^- ions calculated using the pair potential proposed by Catlow *et al* [14] as a function of displacement in the surface-normal direction (z). Here, the relaxed lattice positions determined by MEIS were taken as the origins of the displacements. The calculations were performed using the dipole moments of the top- and second-layer ions

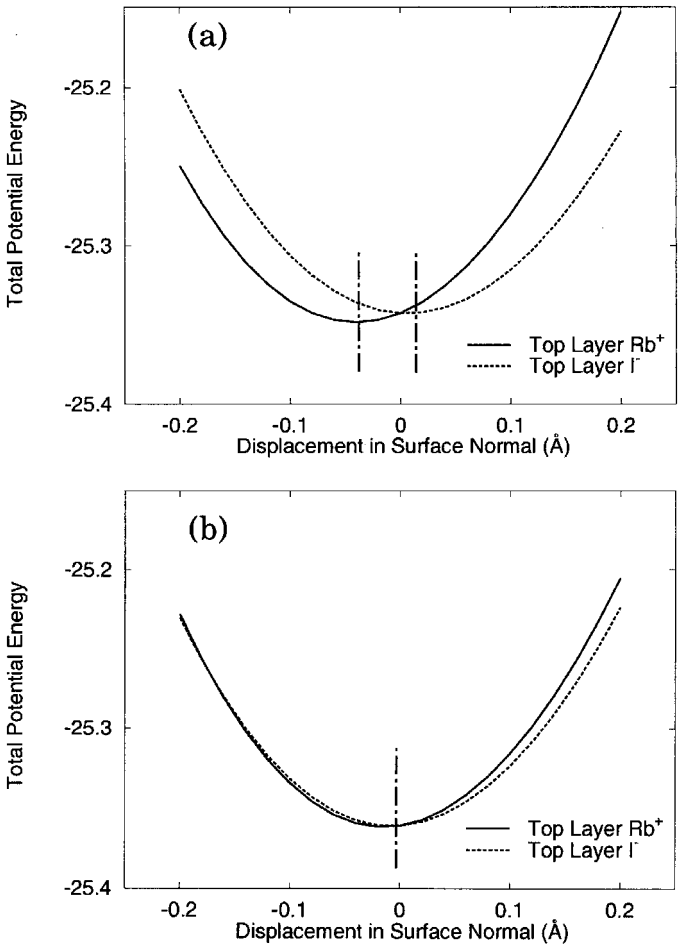

Figure 6. Total potential energies for the top-layer I^- and Rb^+ ions as a function of displacement in the surface-normal direction from the relaxed lattice positions determined by MEIS (a) and from those calculated by MD (b).

determined by MEIS. The displacements and dipole moments of the ions in layers deeper than the third one were neglected because of the very small contributions. The deviations of the equilibrium positions from those determined by MEIS are listed in table 3 for three different polarizabilities [12, 18, 21] and interatomic potentials [12–14]. Here, the minus sign means displacement toward the vacuum side. The discrepancies are small except for in the case using the polarizabilities calculated by Pettersson and Subbaswamy [18], based on first-principles density functional theory. It is worth noting that polarization of an ion or atom in solids cannot be defined without ambiguity in a quantum mechanical sense because the wave functions of valence electrons are not localized completely, and overlap each other at unit-cell boundaries [23]. The present result indicates that the polarizabilities derived experimentally [21, 22] and the interatomic potentials of Born–Mayer type [12–14] are applicable. Figure 6(b) shows the total potential energies as a function of displacement (z) from the relaxed lattice positions estimated from the MD (I) simulation. Quite naturally, the force balance holds at the relaxed lattice positions, which are different from those determined by MEIS (see table 1).

Table 3. Deviations of the calculated equilibrium lattice positions of the top-layer Rb^+ and I^- ions from the relaxed lattice positions determined by MEIS. The numbers in the square brackets indicate the references.

			Deviations (Å)		
α^+ (Å^3)	α^- (Å^3)	Ion species	Benson [12]	Catlow [14]	Sangster [13]
1.81 [11]	5.85 [11]	Rb^+	−0.02	−0.03	−0.03
		I^-	+ 0.02	+ 0.0	+ 0.01
1.38 [17]	6.95 [17]	Rb^+	−0.04	−0.05	−0.05
		I^-	+ 0.04	+ 0.02	+ 0.03
1.80 [20]	6.20 [20]	Rb^+	−0.02	−0.03	−0.03
		I^-	+ 0.02	+ 0.0	+ 0.01

4. Summary

The surface relaxation and the rumpling of the top and second layers of RbI(001) were determined by high-resolution MEIS. The present MEIS analysis gives significantly smaller values compared with the predictions of the semi-classical shell models. The discrepancies are possibly caused by their simplified treatments. On the basis of the classical model regarding the lattice site ion as a point charge with a dipole moment, we calculated the local electric fields at the lattice site ions and evaluated the dipole moments for the top- and second-layer Rb^+ and I^- ions self-consistently from the relaxed lattice positions determined by MEIS together with the polarizabilities estimated from the refraction data. From the balance between the short-range force and the long-range coulombic force, we deduced the equilibrium positions of the top- and second-layer ions, which were consistent with those determined by MEIS. This indicates that the polarizabilities derived from refraction data and the short-range pair potential of the Born–Mayer type are applicable.

Acknowledgments

The authors would like to thank Dr K Kobayashi (National Institute for Research into Inorganic Materials) for valuable discussions and comments on the dipole moments induced at alkali halide surfaces. Special thanks are also due to our colleague, Mr S Ohno, for his assistance in the numerical calculations.

References

[1] van Loenen E J, Frenken J W M and van der Veen J F 1985 *Phys. Rev. Lett.* **54** 827
[2] Tromp R M and Reuter M C 1988 *Phys. Rev. Lett.* **61** 1756
[3] Fenter P and Gustafsson T 1988 *Phys. Rev.* B **38** 10 197
[4] Vrijmoeth J, Zagwijn P M, Frenken J W M and van der Veen J F 1991 *Phys. Rev. Lett.* **67** 1134
[5] Kimura K, Ohshima K and Mannami M 1995 *Phys. Rev.* B **52** 5737
[6] Gustafsson T, Garfunkel E, Gusev E P, Haberle P, Lu H C and Zhou J B 1996 *Surf. Rev. Lett.* **3** 1561
[7] Nishimura T, Hoshino Y, Namba H and Kido Y 2000 *Surf. Sci.* **461** 146
[8] LaFemina J P 1996 *Handbook of Surface Science* vol 1, ed W N Unertl (Amsterdam: Elsevier) ch 4
[9] Nishimura T, Ikeda A and Kido Y 1998 *Rev. Sci. Instrum.* **69** 1671
[10] Nishimura T, Ikeda A, Namba H and Kido Y 1998 *Surf. Sci.* **411** L834
[11] Nishimura T, Ikeda A, Namba H, Morishita T and Kido Y 1999 *Surf. Sci.* **421** 273
[12] Benson G C and Claxton T A 1968 *J. Chem. Phys.* **48** 1356
[13] Sangster M J L 1973 *J. Phys. Chem. Solids* **34** 355

[14] Catlow C R A, Diller K M and Norgett M J 1977 *J. Phys. C: Solid State Phys.* **10** 1395
[15] Welton-Cook M R and Prutton M 1977 *Surf. Sci.* **64** 633
[16] de Wette F W, Kress W and Schroeder U 1985 *Phys. Rev.* B **32** 4143
[17] Mahan G D 1986 *Phys. Rev.* B **34** 4235
[18] Pettersson S and Subbaswamy K R 1990 *Phys. Rev.* B **42** 5883
[19] Okazawa T, Ohno S, Hoshino Y, Nishimura T and Kido Y 2001 *Nucl. Instrum. Methods* B **183** 108
[20] Parry D E 1975 *Surf. Sci.* **49** 433
[21] Tessman J R, Kahn A H and Shockley W 1953 *Phys. Rev.* **92** 890
[22] Jaswal S S and Sharma T P 1973 *J. Phys. Chem. Solids* **34** 509
[23] Vanderbilt D and King-Smith R D 1993 *Phys. Rev.* B **48** 4442